MOLECULAR AND CELLULAR BIOLOGY, June 2010, p. 2896–2908 Vol. 30, No. 12
0270-7306/10/$12.00 doi:10.1128/MCB.00028-10

Lin9, a Subunit of the Mammalian DREAM Complex, Is Essential for Embryonic Development, for Survival of Adult Mice, and for Tumor Suppression▽

Nina Reichert,[1]† Sebastian Wurster,[1] Tanja Ulrich,[1] Kathrin Schmitt,[1] Stefanie Hauser,[1] Leona Probst,[1] Rudolf Götz,[2] Fatih Ceteci,[3] Roland Moll,[4] Ulf Rapp,[3] and Stefan Gaubatz[1]*

University of Wuerzburg, Department of Physiological Chemistry I, Biocenter, Wuerzburg, Germany[1]; University of Wuerzburg, Institut fuer Medizinische Strahlenkunde und Zellforschung, Wuerzburg, Germany[2]; Max Planck Institute for Biochemistry, Department of Molecular Biology, Am Klopferspitz 18, D-82152 Martinsried, Germany[3]; and University of Marburg, Institute of Pathology, Marburg, Germany[4]

Received 11 January 2010/Returned for modification 6 March 2010/Accepted 10 April 2010

The retinoblastoma tumor suppressor protein (pRB) and related p107 and p130 "pocket proteins" function together with the E2F transcription factors to repress gene expression during the cell cycle and development. Recent biochemical studies have identified the multisubunit DREAM pocket protein complexes in *Drosophila melanogaster* and *Caenorhabditis elegans* in regulating developmental gene repression. Although a conserved DREAM complex has also been identified in mammalian cells, its physiological function *in vivo* has not been determined. Here we addressed this question by targeting *Lin9*, a conserved core subunit of DREAM. We found that LIN9 is essential for early embryonic development and for viability of adult mice. Loss of *Lin9* abolishes proliferation and leads to multiple defects in mitosis and cytokinesis because of its requirement for the expression of a large set of mitotic genes, such as Plk1, Aurora A, and Kif20a. While *Lin9* heterozygous mice are healthy and normal, they are more susceptible to lung tumorigenesis induced by oncogenic c-Raf than wild-type mice. Together these experiments provide the first direct genetic evidence for the role of LIN9 in development and mitotic gene regulation and they suggest that it may function as a haploinsufficient tumor suppressor.

The retinoblastoma tumor suppressor protein (pRB) and related p107 and p130 "pocket proteins" function together with the E2F transcription factors to regulate gene expression during the cell cycle (7). The identification of evolutionary conserved pocket protein/E2F complexes in *Drosophila melanogaster* has provided new insights into E2F-mediated gene regulation (21, 24). These multisubunit complexes, alternatively called dREAM or Myb-MuvB (MMB), consist of at least eight subunits, including the repressor dE2F2 and one of the two retinoblastoma-related proteins, RBF1 or RBF2. In addition, the complex also contains *Drosophila* dMYB and three Myb-interacting proteins. RNA interference (RNAi)-mediated depletion of several subunits of the complex demonstrated a role in stable repression of developmental genes, although more recent genome-wide studies have found that dREAM/MMB also functions in activation of genes involved in G_2 and mitosis (2, 13, 21, 24).

Remarkably, all subunits of dREAM/MMB, except for dMYB, are related to the *Caenorhabditis elegans* synMuv class B genes that antagonize RAS-induced vulva differentiation (3, 9). Indeed, several synMuv proteins form a multisubunit complex that is highly related to dREAM/MMB (14). Therefore, in analogy to dREAM/MMB, it has been suggested that DRM mainly functions in gene repression during development (14).

We and others recently identified a complex in human cells that is closely related to dREAM and DRM (20, 25, 31, 40). The human complex, alternatively called LINC or human DREAM, consists of a five-protein core module that binds in quiescent cells to the repressors p130 and E2F4. In S phase this binding is lost and B-MYB associates with the complex. The high degree of conservation of the DREAM-like complexes, together with the important roles of the fly and *C. elegans* complexes in gene repression, suggested that the mammalian complex could also be important for developmental gene repression. However, no such function has been reported yet. *In vitro* studies with mammalian cells have shown that human DREAM in association with E2F4 and p130 represses E2F target genes in G_0. Other studies suggested that human DREAM is mainly required for gene activation in G_2 (20, 25, 29, 32, 40). Recently, mice carrying an 84-amino-acid N-terminal deletion of LIN9, a conserved core subunit of DREAM, have been generated (37). However, except for a mild increase in body size, they do not show any obvious phenotype, probably because the small deletion does not generate a complete loss-of-function protein. Thus, the physiological role of the mammalian DREAM complex is still unclear.

In this study we generated constitutive as well as conditional *Lin9* knockout mice to study the physiological role of the DREAM complex *in vivo*. We provide evidence that LIN9 is

* Corresponding author. Mailing address: University of Wuerzburg, Department of Physiological Chemistry I, Biocenter, Wuerzburg, Germany. Phone: (49) 931-31-84138. Fax: 49-931-31-84150. E-mail: stefan.gaubatz@biozentrum.uni-wuerzburg.de.

† Present address: Friedrich Miescher Institute for Biomedical Research, Novartis Research Foundation, Basel, Switzerland.

▽ Published ahead of print on 19 April 2010.

required for early mouse embryogenesis as well as for survival of adult mice because of its essential role for the transcriptional program at mitosis. Moreover, we find that *Lin9* is a haploinsufficient tumor suppressor in a model of lung carcinogenesis driven by oncogenic c-*raf*. By targeting a conserved subunit of mammalian DREAM, we provide the first direct genetic evidence for its essential role in development, proliferation, and gene expression at mitosis and for its role as a tumor suppressor.

MATERIALS AND METHODS

Mice. *Lin9* gene-trapped embryonic stem (ES) cells (RRI306; Baygenomics) were used to generate chimeric mice. *Lin9* heterozygous mice were interbred to generate *Lin9*-deficient embryos. Mice and embryos were genotyped by either Southern blotting or PCR analysis (see below). Surfactant protein C (SP-C) c-*raf* BXB mice have been described elsewhere (18).

Conditionally targeted Lin9 mice. A ~5-kb genomic fragment containing exons 7 to 11 of *Lin9* and flanking regions was PCR amplified and used to generate the targeting construct in four steps. First, a 393-bp fragment containing exon 7 was amplified, flanked with BamHI sites, and cloned into pBS246 (loxP), which contains a loxP-flanked multiple cloning site (38). Second, a 5′ homology arm of 1,509 kb, flanked with EcoRI, was inserted into the vector. Third, the 3′ homology region (3,266 kb), flanked with XbaI and NotI, was cloned into the SpeI and NotI restriction site in the targeting construct. Fourth, the promoterless the β-galactosidase–neomycin (β-geo) selection cassette (27), containing an EN-2 splice acceptor site (SA), an internal ribosome entry site (IRES), and a fusion between the *lacZ* and *neo* genes, was flanked by FLP recombination target (FRT) sites and was inserted into intron 7. The targeting vector was linearized with NotI and electroporated into ES cells (129/SvEvTaq TC-1). ES cells were selected with 200 μg/ml G418. Positive ES cell clones were identified by Southern blotting and were injected into C57BL/6N blastocysts by the service of PolyGene (Rümlang, Switzerland), which gave rise to chimeric animals. Deletion of the β-geo selection cassette was achieved by crossing the heterozygous animals with transgenic mice expressing FLPe recombinase (35). *Lin9*^{fl} mice were crossed with a Cre-deleter strain (42) and with a mouse line ubiquitously expressing a Cre-ER^{T2} transgene (46). Deletion of *Lin9* in *Lin9*$^{fl/f\,l}$ *CreER*^{T2} mice was achieved by three consecutive daily intraperitoneal injections of 1 mg of tamoxifen in peanut oil. Inductions were performed in 8- to 12-week-old mice.

Genotyping of Lin9 gene trap mice. Genomic DNA was digested with BglII, separated on a 0.8% agarose gel, and transferred to Hybond N$^+$ (Amersham). Southern blots were probed with a 332-bp fragment (probe C) generated with PCR using the primers SG634 and SG635. The membrane was prehybridized at 60°C for 60 min with hybridization buffer (ExpressHyb; Clontech). The probe was labeled with [α-^{32}P]dCTP using a random primer DNA labeling kit (Invitrogen), purified with Sephadex G-50 columns (Amersham), and hybridized for 2 h. The membrane was washed once with 3× SSC (1× SSC is 0.15 M NaCl plus 0.015 M sodium citrate)–0.1% SDS at 60°C for 15 min, two times with 1× SSC–0.1% SDS at 60°C for 30 min, and once with 0.2× SSC–0.1% SDS at room temperature. PCR genotyping was performed using the oligonucleotides SG887, SG885, and SG662. To genotype blastocysts, TaqMan quantitative PCR (qPCR) was used. Oligonucleotides to detect β-geo were SG899, SG900, and SG906. For normalization, primers and probes specific for nerve growth factor (NGF) were used: SG895, SG896, and SG907. Primer sequences are listed below.

Genotyping of conditional Lin9 mice and mouse embryonic fibroblasts (MEFs). The PCR strategy to identify the targeted allele, the floxed (fl) allele, or the delta floxed allele (Δfl) is depicted in Fig. 3C, below. The following primers were used: targeted allele, SG893 and SG894; fl allele, SG722 and SG506. SG722 and SG893 were used to simultaneously detect the wild-type (wt), the fl, and the Δfl alleles. PCR was also used to detect the Cre and Flp transgenes using the following primers: Cre, SG926 and SG927; Flp, SG913and SG914.

Mouse embryonic fibroblasts. Primary embryonic fibroblasts were isolated from 13.5 days postcoitum (dpc) embryos as previously described (12). MEFs were cultivated in Dulbecco's modified Eagle's medium (DMEM) supplemented with 10% fetal calf serum (FCS). Deletion of *Lin9* was achieved by treatment with 1 μM 4-hydroxytamoxifen (4-OHT) for 48 h. To render MEFs quiescent, they were incubated in DMEM supplemented with 0.1% fetal bovine serum for 72 h. Reentry into the cell cycle was induced by the addition of 20% fetal bovine serum. 4-OHT at 1 μM was added for the last 48 h of serum starvation. Cells were collected at the indicated time points. For growth curves, MEFs were plated in triplicate in 24-well plates. At the indicated time points, cells were fixed in 10% formalin and stained with crystal violet. The dye was extracted and the optical density determined (43). For flow cytometry, cells were fixed in 80% ethanol and DNA was stained with 69 mM propidium iodide in 38 mM sodium citrate and 100 mg/ml RNase A for 30 min at 37°C. Samples were analyzed on a Beckman Coulter Fc500 instrument.

Immunofluorescence. For bromodeoxyuridine (BrdU) and phospho-H3 staining, cells were fixed in 3% paraformaldehyde, 2% sucrose in phosphate-buffered saline (PBS), permeabilized with 0.2% Triton X-100, and blocked with 5% goat serum for 30 min. For other stainings, cells were fixed for 5 min in ice-cold Methanol Fix [10 mM 2-(*N*-morpholino)ethanesulfonic acid (pH 6.9), 0.1 mM EGTA, 0.1 mM $MgCl_2$, 90% methanol] and blocked for 30 min in 1% bovine serum albumin in PBS at 37°C. Coverslips were incubated for 1 h at room temperature or at 4°C overnight with primary antibodies. Secondary antibodies were diluted 1:700 in PBS and incubated for 2 h at room temperature. Coverslips were stained with 1 μg/ml 4′,6-diamidino-2-phenylindole (DAPI; Sigma) and mounted in IMMU-MOUNT. The following antibodies were used: anti-γ-tubulin (Sigma T3599), antitubulin (Sigma T6074), anti-mouse Ig–Alexa Fluor 488, anti-rabbit Ig–Alexa Fluor 594 (Molecular Probes), anti-BrdU (BD), and anti-phospho-H3 (Cell Signaling).

Histopathology and *in situ* hybridization. Tissues were dissected in PBS, fixed in 4% paraformaldehyde (PFA) in PBS, and embedded in paraffin. To determine the nuclear area of intestinal villus enterocytes, sections were stained with hematoxylin and eosin (H&E) and images analysis was performed with ImageJ. To quantify BrdU incorporation in the intestine, mice were injected with 1 mg BrdU and sacrificed after 2 h. Sections were stained with BrdU antibodies (1:100; Serotec). Twenty-five crypts per mouse were analyzed (three mice for each time point). For quantification of lung tumor size in SP-C c-*raf* BXB animals, at least eight animals per genotype were analyzed. The number of tumor foci was calculated from whole lung sections with a cutoff of >0.01 mm^2 for tumor area. RNA *in situ* hybridization was performed as described previously (23).

Immunohistochemistry. Sections were deparaffinized and rehydrated. After 15 min of incubation with 3% H_2O_2 to quench endogenous peroxidase, sections were boiled in 10 mM sodium citrate buffer (pH 6.0) for 10 to 15 min for antigen retrieval. Slides were blocked with serum containing 0.1% Triton X-100 in PBS and incubated with relevant primary antibodies overnight at 4°C. Biotinylated secondary antibodies (Dako Cytomation) were applied to sections at 1:200 and incubated for 60 min at room temperature. ABC reagent (Vectastain Elite ABC kit; Vector Labs) was applied to sections and developed in diaminobenzidine (DAB). Slides were then counterstained with hematoxylin. The antibodies used were as previously described (34).

Isolation and *in vitro* culture of blastocysts. Blastocysts were collected from pregnant mice at 3.5 dpc and grown in ES cell medium (DMEM, 10% FCS, 1% penicillin-streptomycin, 1% nonessential amino acids, 50 μM β-mercaptoethanol, 0.12% leukemia-inhibitory factor) in four-well plates (Multidish 4SI; Nunc) coated with 0.2% gelatin–PBS at 37°C and 5% CO_2 and monitored every 24 h. To isolate genomic DNA, blastocysts were transferred through several drops of PBS, incubated for 2 h at 65°C in 2 μl tail buffer (100 mM Tris-Cl [pH 8.5], 5 mM EDTA, 0.2% SDS, 200 mM NaCl, 250 mg/ml proteinase K), and heat inactivated at 95°C for 10 min. To isolate genomic DNA from cultured blastocysts or paraffinated fixed 7.5-dpc embryos on sections, NucleoSpin columns (Macherey-Nagel) for small tissue samples were used. Genotyping was performed with TaqMan qPCR.

Immortalization of MEFs and transformation assays. Early passage (p2) *Lin9*$^{fl/+}$ *CreER*^{T2} MEFs were infected with retroviral expression constructs encoding simian virus 40 (SV40) large T or large T(Δ89–97) as described previously (5, 11). After selection with 400 μg/ml neomycin for 10 days, cells were split and treated with 400 nM 4-OHT for 48 h or left untreated. At 18 to 24 h after OHT removal, 1×10^5 cells were transferred to 2 ml DMEM containing 0.35% low-gelling agarose and seeded in triplicate into six-well plates containing a 2-ml layer of solidified 0.7% agarose in complete medium. After 10 days, the number of foci was determined. Only foci with a diameter greater than 40 μm were counted. The number of foci per square centimeter was determined.

Time-lapse microscopy. For live cell imaging, *Lin9*$^{fl/fl}$ *CreER*^{T2} MEFs were infected with a retrovirus encoding H2B-enhanced green fluorescent protein (EGFP). Cells were grown in 35-mm μ-Dish chambers (Ibidi, Munich, Germany) and treated with 400 μM 4-OHT for 48 h. Live cell imaging was performed using a Leica heating insert with attached incubator (S-2). Images were captured every 5 to 6 min using the Leica Application Suite. Images were processed using ImageJ.

RT-PCR. Total RNA was isolated with Trizol (Invitrogen), reverse transcribed with 0.5 units of Moloney murine leukemia virus reverse transcriptase (RT; Promega), and analyzed by quantitative real-time PCR with SYBR green reagents from Thermo Scientific using the Mx3000 (Stratagene) detection system.

Expression differences were calculated as described before (40). The sequences of the primers used are listed below.

Western blotting and immunoprecipitation. Whole-cell lysates from MEFs were immunoprecipitated overnight at 4°C with anti-LIN9 antiserum (11). Immunoprecipitates were collected on protein A-Sepharose and washed five times with 50 mM Tris (pH 7.5)–120 mM NaCl–5 mM EDTA–0.5% NP-40. Proteins were separated by SDS-gel electrophoresis and transferred to a polyvinylidene difluoride membrane. Proteins were detected by immunoblotting.

ChIP. Chromatin immunoprecipitation (ChiP) assays were performed as described before (40). Enrichment of DNA was analyzed by quantitative real-time PCR. Primer sequences are listed below.

Microarray analysis. RNA from 4-OHT-treated *Lin9*$^{fl/fl}$ MEFs was hybridized against RNA from mock-treated cells. One hundred nanograms of total RNA was amplified and labeled using the two-color Quick-Amp labeling kit (Agilent), hybridized to a 44K mouse oligo array (Agilent), and analyzed as described before (19). Expression data and gene annotations were stored in Array Express (http://www.ebi.ac.uk/arrayexpress/, under accession number E-MEXP-2097), which complies with MIAME (minimal information about a microarray experiment) guidelines.

Primer sequences. Primers to generate the Southern blotting probe C were SG634, 5′-TGC TGT GTA GCC TCA GAT GG-3′, and SG635, 5′-CCA GCT TTT CTG CTT CTG TG-3′. Primers and probes for TaqMan qPCR included the following: three for β-geo, SG899, 5′-CGG TCG CTA CCA TTA CCA GT-3′, SG900, 5′-CGT GCA ATC CAT CTT GTT CA-3′, and SG906, 5′–6-carboxyfluorescein–TCA TAT TGG CTG CAG CCC GGG–Black Hole Quencher 1 (BHQ-1); three for NGF, SG895, 5′-TGC ATA GCG TAA TGT CCA TGT TG-3′, SG896, TCT CCT TCT GGG ACA TTG CTA TC-3′, and SG907, 5′–6-carboxy-2′,4,4′,5′,7,7′-hexachlorofluorescein–ACG GTT CTG CCT GTA CGC CGA TCA–BHQ-1–3′. Primers for genotyping of *lin9* alleles included the following: SG887, 5′-TAA AGT GTG GCC CAT CAC AA-3′; SG885, 5′-CCC ACT GAC CAG AAG GAA AG-3′; SG662, 5′-CCT GCT AGT CTA AAA TTT CTT TTG GT-3′; SG893, 5′-CCT GGC TGC CTA GCA TTT AC-3′; SG894, 5′-CCA GGC CAG GCT AAC ATT AC-3′; SG722, 5′-GCA AAA GCT GCA AGT CCT CT-3′; SG506, 5′-AGT CTT GCC TGC ACA GGG A-3′.

Primers for detection of transgenes. Primers for detection of Cre transgenes were SG926, 5′-GGCATTTCTGGGGATTGC-3′, and SG927, 5′-CAGACCAG GCCAGGTATCTC-3′. For detection of the Flp transgene, SG913, 5′-CACTG ATATTGTAAGTAGTTTGC-3′, and SG914, 5′-CTAGTGCGAAGTAGTGA TCAGG-3′, were used.

Primer sequences for RT-qPCR. Primers for RT-qPCR for Lin9 were SG785, 5′-TTGGGACTCACACCATTCCT-3′, and SG786, 5′-GAAGGCCGCTGTTT TTGTC-3′. Primers for Nusap1 were SG1030, 5′-TCTAAACTTGGGAACAA TAAAAGGA-3′, and SG1031, 5′-TGGATTCCATTTTCTTAAAACGA-3′. For Aspm, SG1026, 5′-GATGGAGGCCGAGAGAGG-3′, and SG1027, 5′-CA GCTTCCACTTTGGATAAGTATTTC-3′ were used. Cenpf primers were SG1038, 5′-AGCAAGTCAAGCATTTGCAC-3′, and SG1039, 5′-GCTGCTTC ACTGATGTGACC-3′. Addition primers were as follows: for Plk1, SG1028, 5′-TTGTAGTTTTGGAGCTCTGTCG-3′, and SG1029, 5′-AGTGCCTTCCTC CTCTTGTG-3′; for Cenpe, SG1198, 5′-TCTTTACCGTCTGAGGTGGAA-3′, and SG1199, 5′-GGAGCTCTTCAGATTTCTCATACA-3′; for Kif20a, SG1200, 5′-AAGGACCTGTTGTCAGACTGC-3′, and SG1201, 5′-TGAGGTGTCCTC CAGTAGAGC-3′; for Hmmr, SG1202, 5′-TCACGGAGTCTAAGGGAAAAA T-3′, and SG1203, 5′-TTCATCGATCTTTTCTTTCTCTATTG-3′; for Aurka, SG1009, 5′-GGGACATGGCTGTTGAGG-3′, and SG1010, 5′-GTTTTCTTTA CATCTGTCCATGTCA-3′; for Mybl2, SG820, 5′-TTAAATGGACCCACGAG GAG-3′, and SG821, 5′-TTCCAGTCTTGCTGTCCAAA-3′; for Mcm8, SG1178, 5′-TGGAAAATACACCCTTCCTACAA-3′, and SG1179, 5′-GCAGT GGAGCAAATGACCTC-3′; for Fancg, SG1118, 5′-CCTGCTAGCAAGTCG ATGC-3′, and SG1119, 5′-AGGTCCAGGTAATGCTCTGC-3′; for Rad18, SG1120, 5′-AAGGAAATTGAGGAAGTTCACAGT-3′, and SG1121, 5′-CAT CGCTGCAGCTTGTGA-3′; for Rad51, SG1122, 5′-CGAGGGTTCAACACA GACC-3′, and SG1123, 5′-AGGGCAGTAGCACTGTCTACAA-3′; for Fancb, SG1124, 5′-GAAAATTATTATTTGGTGCTTCCAG-3′, and SG1125, 5′-GAG ATATGCTGCTGGATTTTGTT-3′; for Ercc6l1, SG1194, 5′-AAGATATGGA GGAAAGGCTTGA-3′, and SG1195, 5′-TCTGAAAGCCCTGGCTCA-3′; for Hprt, SG783, 5′-TCCTCCTCAGACCGCTTTT-3′, and SG784, 5′-CCTGGTT CATCATCGCTAATC-3′.

Primer sequences for ChIP. For ChiP experiments, the primers included the following: for Aspm, SG1050, 5′-GCTGTAGCGAGGAGGTTCC-3′, and SG1051, 5′-TTTTGCTCGGTTCAAATATCG-3′; for Kif20a, SG1207, 5′-CAG ACAGTCTTCGGGTGAGTG-3′, and SG1208, 5′-CTTCTACGGACGCGCA AG-3′; for glyceraldehyde-3-phosphate dehydrogenase (GAPDH), SG976, 5′-A TTTCCCCTGTTCTCCCATT-3′, and SG977, 5′-GACATCCAGGACCCAG AGAC-3′.

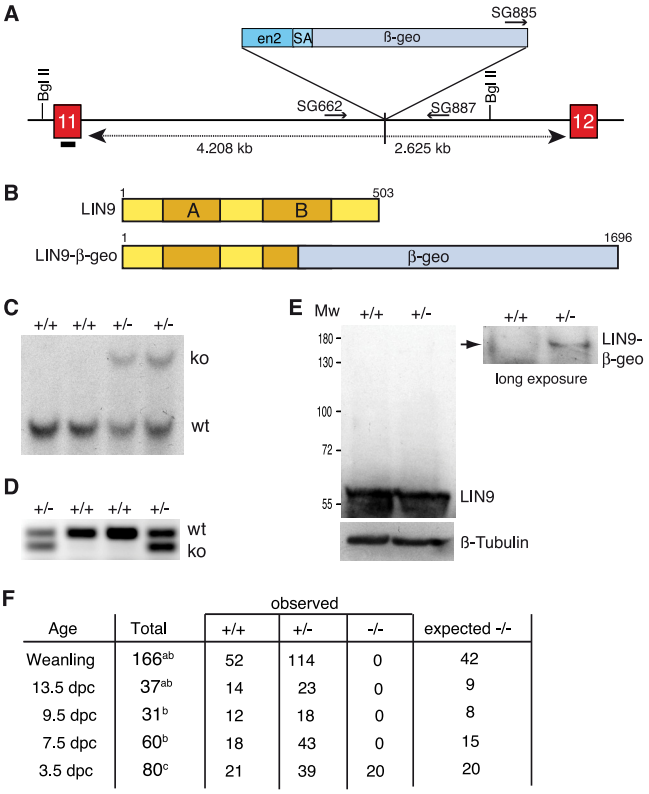

F

Age	Total	observed +/+	observed +/-	observed -/-	expected -/-
Weanling	166[ab]	52	114	0	42
13.5 dpc	37[ab]	14	23	0	9
9.5 dpc	31[b]	12	18	0	8
7.5 dpc	60[b]	18	43	0	15
3.5 dpc	80[c]	21	39	20	20

FIG. 1. Early embryonic lethality of *Lin9* mutant mice. (A) Schematic diagram of the *Lin9* wild-type locus and the trapped allele. PCR primers for genotyping are also shown. (B) The gene trap insertion leads to a C-terminally truncated LIN9 protein fused to the β-galactosidase-neomycin marker. (C) Southern blot analysis of BglII-digested genomic DNA from wild-type and heterozygous mice. (D) PCR to detect the *Lin9* wild-type and knockout alleles in genomic DNA from tail biopsy specimens with primers SG662, SG885, and SG887. The primer pair SG662 and SG887 is specific for the wild-type allele. SG885 and SG887 detect the knockout allele. The position of the primers is indicated in panel A. (E) Western blot analysis showing the expression of LIN9 and the LIN9–β-geo fusion protein in *Lin9*$^{+/-}$ testes. A fusion protein of the expected molecular weight could be detected in *Lin9* heterozygous (*Lin9*$^{+/-}$) mice, but it was expressed at very low levels and was only detected after long exposure of the blot. (F) Embryonic lethal phenotype of homozygous *Lin9* knockout mice. Outcomes for progeny arising from intercrosses of *Lin9*$^{+/-}$ animals are shown. Footnotes indicate that genotypes were determined by Southern blotting (a), PCR (b), or TaqMan qPCR (c).

RESULTS

Lin9 is required for early mouse development. To determine the role of LINC/DREAM in mammalian development, we generated *Lin9* mutant mice using an embryonic stem cell line containing a gene trap vector inserted in the *Lin9* locus (Fig. 1A to E). The gene trap insertion leads to a C-terminally truncated Lin9 protein fused to the β-geo resistance marker. Because this disrupts the evolutionarily conserved B-box of Lin9, the gene trap fusion is predicted to produce a nonfunctional protein. A fusion protein of the expected molecular weight could be detected in *Lin9* heterozygous mice, but it was

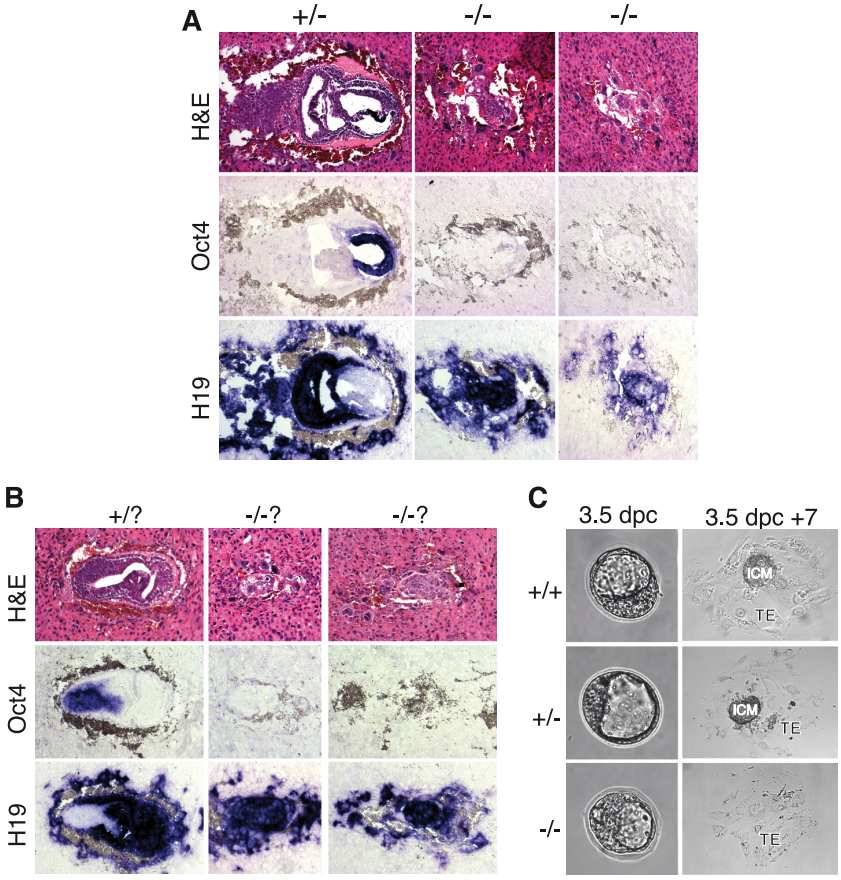

FIG. 2. *Lin9*$^{-/-}$ embryos lack the epiblast, and the ICM of *Lin9*$^{-/-}$ blastocysts is not maintained in culture. (A) Histological sections of deciduae from heterozygous *Lin9*$^{+/-}$ breedings at day 7.5 dpc were stained with H&E. Also shown are results of *in situ* hybridization for Oct4 and H19. About one-quarter (10 out of 48) of embryos displayed abnormal morphology. Genotyping confirmed that they were of the *Lin9*$^{-/-}$ genotype. (B) Deciduae from 6.5 dpc mice were stained with H&E and used for *in situ* hybridization of Oct4 and H19. Twelve out of 59 embryos were highly abnormal and were presumably of the *Lin9*$^{-/-}$ genotype. (C) Phase-contrast microscopy of blastocysts isolated from *Lin9*$^{+/-}$ intercrosses and cultured for 7 days. *Lin9*$^{-/-}$ and *Lin9*$^{+/-}$ blastocysts hatched from their zona pellucidae. The trophectoderm (TE) attached to and spread out at the bottom of wells. The ICM underwent proliferation. Homozygotes hatched and initially formed TE and ICM; however, the ICM was not maintained.

expressed at very low levels (Fig. 1E). Heterozygous *Lin9*$^{+/-}$ mice developed normally, were fertile, and showed no obvious defects (data not shown). However, no homozygous *Lin9*$^{-/-}$ mice were found from intercrosses between heterozygous mice, indicating that disruption of *Lin9* results in embryonic lethality (Fig. 1F). To determine the time of *Lin9*$^{-/-}$ lethality, we genotyped embryos from heterozygous intercrosses. At the blastocyst stage, *Lin9*$^{-/-}$ embryos were detected with the expected frequency. However, genotyping of embryos dissected from the deciduae at embryonic days 7.5 to 13.5 revealed that none of the embryos was *Lin9*$^{-/-}$. Partially resorbed embryos that could not be genotyped were evident at these time points, suggesting that *Lin9*$^{-/-}$ embryos die shortly after implantation.

Next, we analyzed histological sections of decidual swellings obtained from crosses of *Lin9*$^{+/-}$ mice at embryonic days 6.5 and 7.5. At day 7.5, about 25% of the embryos had severe phenotypic abnormalities and lacked the typical epithelial cells of the epiblast (Fig. 2A). Similarly, at day 6.5, about 25% of the embryos were highly abnormal and had not developed the three germ layers, the amnion, chorion, and allantois (Fig. 2B). The frequency of about 25% of abnormal embryos suggests that they are Lin9 null. Indeed, PCR genotyping with genomic DNA isolated from histological sections of abnormal embryos at day 7.5 dpc confirmed that they were of the Lin9$^{-/-}$ genotype (data not shown). RNA *in situ* hybridization for Oct4 stained the epiblast of wild-type embryos, as expected (28) (Fig. 2A and B). However, no Oct4 staining was detected in *Lin9*$^{-/-}$ implantation sites. In contrast, H19, which is expressed in all extraembryonic cell types in normal implantation sites (33), gave a signal through the entire area of implantation sites of *Lin9*$^{-/-}$ embryos. Together these observations indicate that *Lin9*$^{-/-}$ embryos do implant but that cell types that are derived from the inner cell mass (ICM) are not maintained after implantation.

To analyze the phenotype of Lin9 embryos before implantation, blastocysts were obtained from heterozygous crosses and cultured *in vitro* in ES cell medium. Embryos were monitored for 7 days in culture and then genotyped. Both wild-type and *Lin9*$^{-/-}$ embryos hatched from their zona pellucida (Fig. 2C). After hatching, most wild-type (11 of 13) and heterozygous (21 of 23) blastocysts outgrew a layer of trophoblast giant

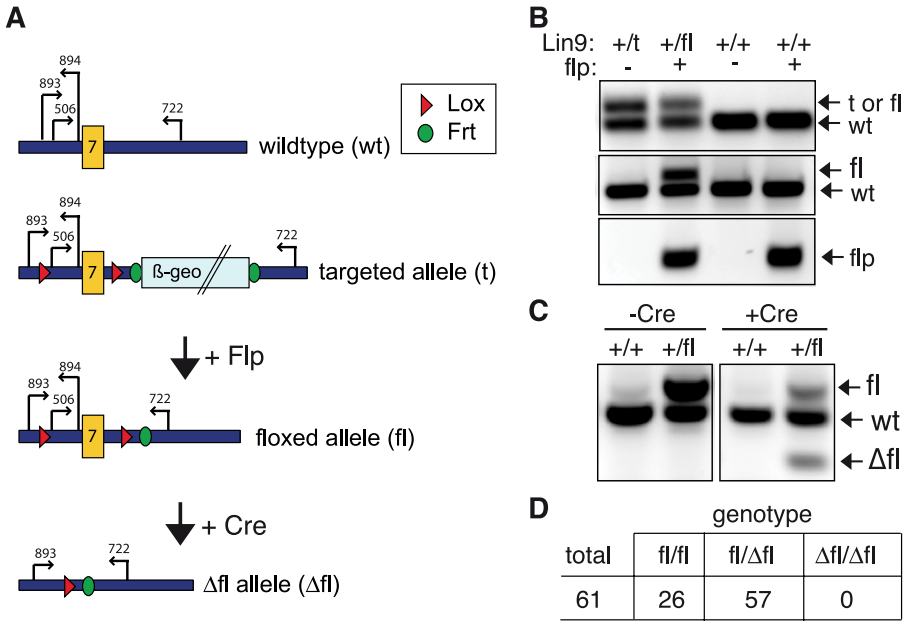

FIG. 3. A conditional allele of *Lin9*. (A) Schematic diagram of the wild-type *Lin9* locus and the targeted allele. Flp-mediated deletion of the selection cassette results in the floxed allele (fl), and Cre-mediated deletion of exon 7 results in the knockout (Δfl) allele. Correct targeting of *Lin9* was verified by Southern blotting (data not shown). The locations of primers used for PCR genotyping are indicated. (B) Deletion of the selection cassette from the targeted *Lin9* locus *in vivo* was achieved by crossing to a mouse strain carrying a *flp* transgene. Results shown are from PCR genotyping of tail DNA from crosses of $Lin9^{+/t}$ mice with *flp* transgenic mice to detect the wt, targeted (t), and the floxed (fl) alleles with primers SG893 and SG894 (top panel). Primers SG506 and SG722 were used to detect the wt and fl alleles (middle panel). The bottom panel shows a Flp-specific PCR with primers SG913 and SG914 to verify the presence of the Flp transgene. (C) $Lin9^{fl/+}$ animals were crossed to mice ubiquitously expressing Cre recombinase. PCR genotyping of tail DNA with primers SG722 and SG893 was used to detect the wt, fl, and Δfl alleles. (D) $Lin9^{\Delta fl}$ results in lethality at homozygosity. $Lin9^{\Delta fl/fl}$ mice were intercrossed. Genotypes of progeny were determined by PCR.

cells with a robust ICM on top. *Lin9* mutant blastocysts initially also formed a trophoblast monolayer with ICM. However, the ICM of most $Lin9^{-/-}$ embryos failed to expand, and by day 7 in culture the ICM of 11 of 12 $Lin9^{-/-}$ embryos was lost (Fig. 2C). Together these data indicate that *Lin9* is required for the viability of the ICM *in vitro* and for the maintenance of the epiblast *in vivo*.

A conditional allele of Lin9. To circumvent the early embryonic lethality and to investigate the effect of loss of *Lin9* in adult mice and in MEFs, we generated a conditional allele of *Lin9*. Using homologous recombination, we flanked exon 7, which encodes part of the conserved box A of LIN9, with loxP sites (Fig. 3A). A neomycin selection cassette flanked by FRT sites was placed into the intron after exon 7 and was removed *in vivo* by breeding to transgenic mice expressing the Flp recombinase (Fig. 3B). The resultant $Lin9^{fl}$ allele could be bred to homozygosity, indicating that it encodes a functional protein. Exon 7 was efficiently removed *in vivo* by crossing to mice of a Cre-deleter strain ($Lin9^{\Delta fl}$ allele) (Fig. 3C). $Lin9^{\Delta fl}$ resulted in embryonic lethality at homozygosity, indicating that $Lin9^{\Delta fl}$ is a null allele and confirming the results obtained with the $Lin9^{-/-}$ allele (Fig. 3D).

Loss of Lin9 causes various defects in mitosis. To investigate the role of *Lin9* in MEFs, we crossed $Lin9^{fl}$ animals with a mouse line ubiquitously expressing a $CreER^{T2}$ transgene, which can be activated by 4-OHT. Next, we prepared MEFs from $Lin9^{+/+}$ and $Lin9^{fl/fl}$ embryos containing $CreER^{T2}$. Upon treatment of early passage $Lin9^{fl/fl}$ $CreER^{T2}$ MEFs with 4-OHT, exon 7 was successfully deleted and *Lin9* mRNA and protein levels were strongly reduced (Fig. 4A, B, and C). Proliferation of 4-OHT-treated $Lin9^{fl/fl}$ $CreER^{T2}$ MEFs was severely impaired, whereas 4-OHT had no effect $Lin9^{+/+}$ $CreER^{T2}$ MEFs (Fig. 4D). To better understand the nature of the cell cycle defect, we next analyzed reentry into the cell cycle from quiescence. 4-OHT was added to serum-starved $Lin9^{+/+}$ and $Lin9^{fl/fl}$ MEFs containing $CreER^{T2}$. Cell cycle reentry was induced by addition of serum. S phase and mitosis were monitored by BrdU incorporation and by staining for phosphorylated histone H3, respectively (Fig. 4E and F). Like their wild-type counterparts, *Lin9* mutant cells arrested normally in a low serum concentration (Fig. 4E). They also entered into S phase with virtually normal kinetics after serum stimulation, indicating that LIN9 is dispensable for growth arrest after serum removal and for timely reentry into S phase. Entry into mitosis of *Lin9* mutant MEFs was delayed by approximately 3 h, indicating a modest G_2 delay in *Lin9*-deficient cells (Fig. 4F).

Although *Lin9* mutant MEFs reentered with relatively normal kinetics into the first cell cycle, their fluorescence-activated cell sorting (FACS) profiles looked highly abnormal already at 24 h after serum stimulation. At 48 h after serum addition, a large proportion of cells with a DNA content of $>4n$ were present in *Lin9*-deficient MEFs (Fig. 4G). Microscopic examination showed a high proportion of cells with aberrant nuclei. Abnormalities observed include an increase in binuclear cells from 2.5% to over 20%, micronucleation, nuclei with multiple lobes, and doughnut-shaped nuclei (Fig. 4H and I). BrdU labeling demonstrated ongoing DNA synthesis at reduced levels in these aberrant nuclei, consistent with the increased DNA

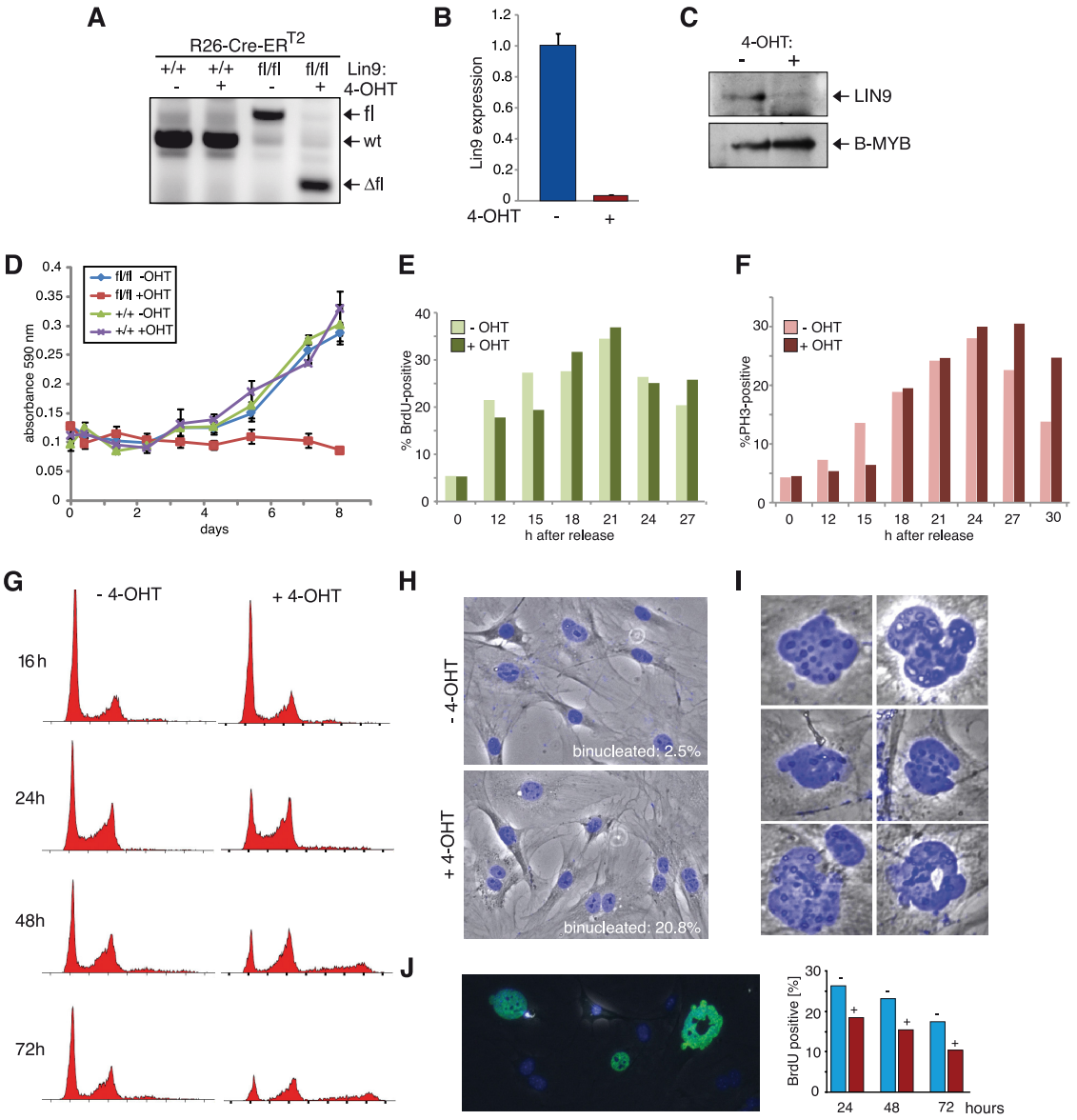

FIG. 4. Impaired proliferation of *Lin9*-deficient MEFs. (A) MEFs isolated from embryos with the indicated genotypes were treated with 4-OHT. The genotype was determined by PCR. (B and C) Reduction of Lin9 mRNA and protein levels in 4-OHT-treated MEFs as determined by RT-qPCR and immunoblotting, respectively. B-MYB protein levels are also shown and were unchanged. (D) Impaired proliferation of *Lin9*-deficient MEFs. *Lin9*$^{+/+}$ *CreER*^{T2} and *Lin9*$^{fl/fl}$ *CreER*^{T2} MEFs were treated with 4-OHT where indicated, and growth was analyzed. (E) *Lin9*$^{fl/fl}$ *CreER*^{T2} MEFs were made quiescent by serum starvation. At 24 h after serum removal, 4-OHT was added, as indicated. Forty-eight hours later, reentry into the cell cycle was induced by addition of 20% serum and was monitored by BrdU incorporation. (F) Entry into mitosis of the indicated MEF cultures was analyzed by staining with an antibody specific for phosphorylated histone H3. The experiment shown in panels E and F has been repeated several times. One representative experiment is shown. (G) *Lin9*$^{fl/fl}$ *CreER*^{T2} MEFs were treated with 4-OHT for 48 h. At the indicated time points after 4-OHT treatment, the cell cycle profile was determined by flow cytometry. (H) Binucleated cells in 4-OHT-treated *Lin9*$^{fl/fl}$ *Cre-ER*^{T2} MEFs. The percentage of binucleated cells was determined by DAPI staining and fluorescence microscopy. (I) Examples of nuclear abnormalities observed upon deletion of *Lin9*. Cells were stained with DAPI and analyzed by fluorescence microscopy. (J) Ongoing DNA synthesis upon deletion of *Lin9*. *Lin9*$^{fl/fl}$ *CreER*^{T2} MEFs were treated or not with 4-OHT for 48 h. At the indicated time points thereafter, DNA synthesis was quantified by BrdU incorporation. The left panel shows abnormal morphology of BrdU-positive nuclei (green) at 48 h after 4-OHT treatment. The right panel shows the percentage of BrdU-positive cells at the indicated time points.

content in the FACS profiles (Fig. 4J). Reexpression of LIN9 in *Lin9*$^{fl/fl}$ *CreER*^{T2} MEFs rescued the *Lin9* mutant phenotype, indicating that it is not the result of secondary genetic effects or of Cre-mediated toxicity (data not shown).

To monitor progression through mitosis and chromosome segregation in individual cells, we performed time-lapse video microscopy using H2B-EGFP to label the chromatin. While most untreated cells exhibited normal mitosis, we observed multiple types of mitotic errors, such as chromatin bridges, failed nuclear segregation, and cytokinesis failure after deletion of *Lin9* (Fig. 5A and data not shown). These defects frequently resulted in binucleated and tetraploid cells with

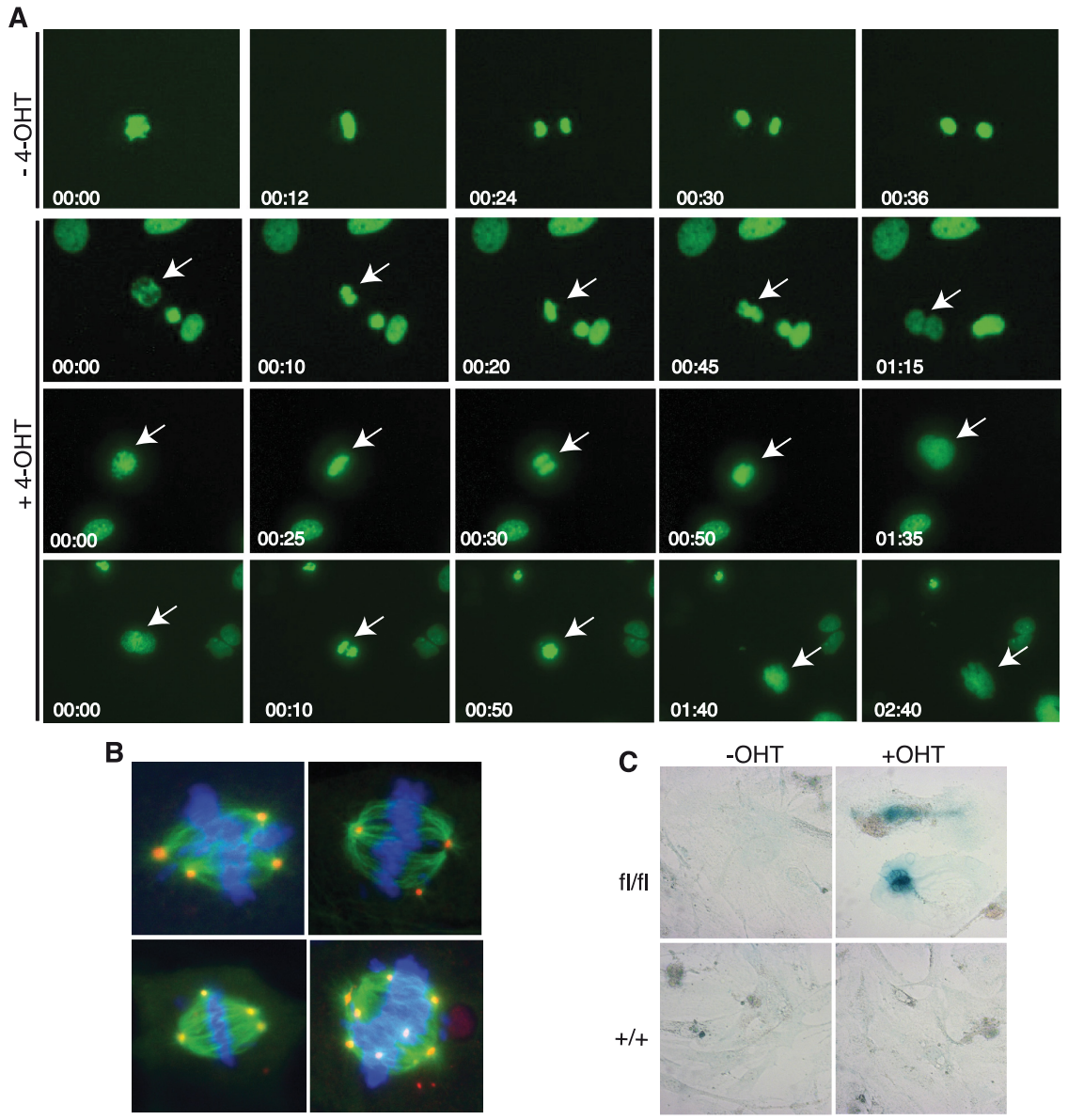

FIG. 5. Mitotic phenotype and senescence of LIN9-deficient MEFs. (A) H2B-EGFP was expressed in *Lin9*$^{fl/fl}$ *CreER*^{T2} MEFs treated with or without 4-OHT. Images were recorded by time-lapse microscopy. Selected frames from the time-lapse videos are shown. The arrows point to cells whose mitosis or cytokinesis was abnormal. (B) Multipolar spindles after deletion of *Lin9*. Cells were stained with antibodies directed against α-tubulin (green) and γ-tubulin (red) to detect mitotic spindles and centrosomes, respectively. DNA was counterstained with DAPI (blue). (C) Senescence of *Lin9*-deficient MEFs. Early-passage primary *Lin9*$^{fl/fl}$ *CreER*^{T2} MEFs were treated with 4-OHT as indicated. Two weeks after 4-OHT treatment, *Lin9*$^{fl/fl}$ *CreER*^{T2} MEFs were stained for SA–β-gal, a marker of senescent cells. Phase-contrast images are shown.

large and highly abnormal nuclei, indicating that LIN9 is required for proper mitosis and cytokinesis. By 72 h after 4-OHT removal 38% of mitoses showed chaotic multipolar spindles and supernumary centrosomes (Fig. 5B). In contrast, only 6% of mitoses were abnormal in untreated MEFs. After 2 weeks in culture a significant proportion of *Lin9* mutant cells exhibited a large and flat morphology and stained positive for senescence-associated β-galactosidase activity (Fig. 5C). Importantly, at this time point, no senescence was detected in untreated *Lin9*$^{fl/fl}$ MEFs of the same passage or in 4-OHT-treated *Lin9*$^{+/+}$ CreER^{T2} MEFs.

In conclusion, we observed multiple defects in *Lin9* mutant MEFs, including a moderate delay in mitotic entry, tetraploidization, formation of multipolar spindles, and centrosome amplification. These phenotypes are suggestive of defects in spindle assembly, chromosome segregation, and cytokinesis. The mitotic defects ultimately result in premature senescence of *Lin9* mutant cells.

Role of LIN9 in gene regulation. We next asked whether the mitotic defects of *Lin9* mutant cells are caused by transcriptional defects. RNA was isolated from *Lin9*$^{fl/fl}$ *CreER*^{T2} MEFs treated with or without 4-OHT and was subjected to Agilent DNA microarrays, monitoring more than 41,000 transcripts. Deletion of *Lin9* resulted in significant upregulation and down-

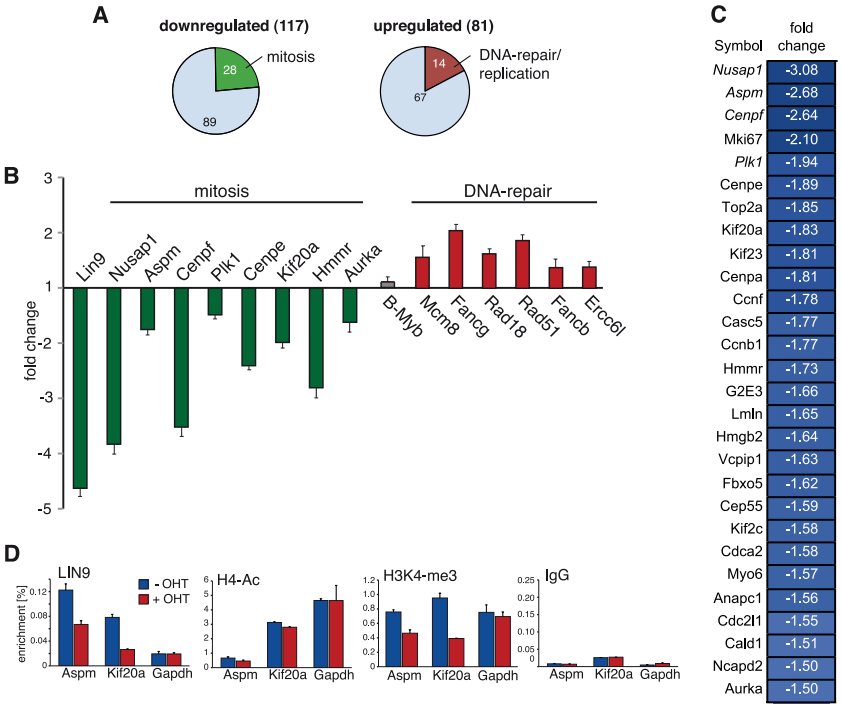

FIG. 6. *Lin9* target genes. (A) Transcriptional profiling of *Lin9* knockout MEFs. RNA was isolated from $Lin9^{fl/fl}$ $CreER^{T2}$ MEFs treated with or without 4-OHT for 48 h. Genome-wide microarray analysis was used to identify LIN9-regulated genes. Expression data were stored in Array Express (http://www.ebi.ac.uk/arrayexpress/; accession number E-MEXP-2097). (B) RT-qPCR was used to confirm up- and downregulation of the indicated genes upon deletion of *Lin9*. (C) Genes downregulated after deletion of *Lin9* with a known function in mitosis. (D) ChIP analysis of the indicated promoters with chromatin isolated from untreated and 4-OHT-treated $Lin9^{fl/fl}$ $CreER^{T2}$ MEFs. Bound DNA was analyzed by qPCR.

regulation of many genes, indicating functions for LIN9 in gene repression and activation (Fig. 6A). LIN9-dependent regulation of selected genes from the microarray analysis was confirmed by quantitative PCR (Fig. 6B). Genes that were upregulated in the absence of LIN9 and thus require LIN9 for repression encode diverse cellular functions, such as signal transduction and transcription. A fraction of the upregulated genes (17%) encode proteins with roles in DNA repair and recombination, such as Rad18, Mcm8, Mutyh, Blm, and Fanci (Fig. 6A). Genes that were downregulated in the absence of LIN9 also play roles in diverse cellular functions. Significantly, a large fraction of the downregulated genes (24%) have a known function in mitosis and cytokinesis (Fig. 6C). Mitotic genes that were downregulated in *Lin9*-deficient MEFs included *Aspm*, *Nusap1*, and *Cenp-f*; *Cenp-e*; and *Kif20a* (*Mklp2*) and *Cep55*, which are involved in chromosome segregation, the mitotic checkpoint, and in cytokinesis, respectively. Downregulation of these mitotic genes could be responsible, at least in part, for the mitotic phenotype and the nuclear abnormalities observed after deletion of *Lin9*.

ChIP experiments confirmed binding of LIN9 to the promoters of the mitotic genes Aspm and Kif20a (Fig. 6D). Binding of LIN9 to these promoters was reduced after deletion of *Lin9* by treatment of MEFs with 4-OHT. Reduced binding of LIN9 correlated with decreased mitotic gene expression. After deletion of *Lin9*, lysine 4 trimethylation of histone H3 (H3K4-me3) was decreased, consistent with the proposed role of this modification in gene activation (4, 41). In contrast, there was little effect on acetylation of histone H4. In summary, deletion of *Lin9* resulted in downregulation of mitotic genes, and this could be responsible, at least in part, for the mitotic phenotype and the nuclear abnormalities observed after deletion of *Lin9*.

Lin9 deletion in adult mice leads to rapid mortality and to loss of intestinal epithelium. Next we investigated whether *Lin9* is also required for proliferation *in vivo*. To address this possibility Lin9 was deleted in somatic cells of adult $Lin9^{fl/fl}$ $CreER^{T2}$ mice by tamoxifen injection. PCR genotyping showed efficient recombination in the gastrointestinal tract, liver, kidney, testis, and spleen (Fig. 7A). Moderate levels of recombination were detected in all other tissues tested. The only tissue that lacked recombination was the brain. Treatment of $Lin9^{fl/fl}$ $CreER^{T2}$ mice with tamoxifen for 3 days had a dramatic effect: all treated mice died within 7 days of the first tamoxifen injection, indicating that LIN9 is critically required for survival of mature mice. Importantly, tamoxifen had no effect on the survival of $Lin9^{+/+}$ $CreER^{T2}$ mice. Histological analysis of the small intestine, which renews in the mouse every 3 to 5 days, demonstrated a dramatic atrophy of this tissue after *Lin9* deletion: more than 80% of the villus epithelium was lost 6 days after the first tamoxifen injection, whereas the intestine of tamoxifen-treated control mice was unaffected (Fig. 7B). No increase in abundance of apoptotic cells was observed (data not shown). However, *Lin9*-deficient crypts showed a reduced number of cells that stained positive for the proliferation marker Ki67, indicating defects in cell cycle progression (Fig. 7C). Reduced cell cycle proliferation was confirmed by labeling cells in S phase with BrdU (Fig. 7D). In wild-type mice, a 2-hour pulse of BrdU labeled approximately six to seven cells

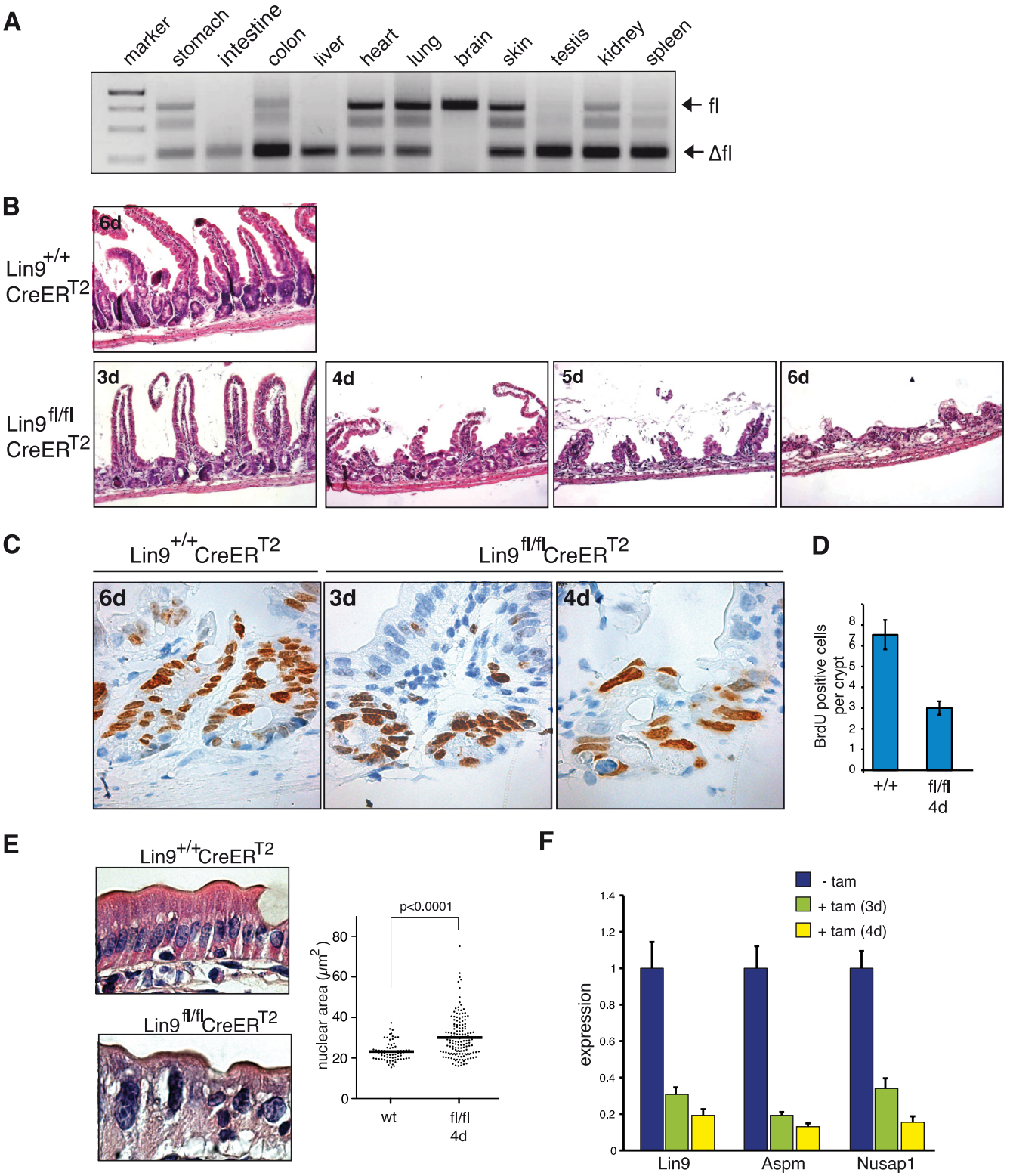

FIG. 7. Loss of *Lin9* in adult mice leads to rapid loss of proliferating intestinal epithelial cells. (A) Inducible deletion of *Lin9* in adult mice. (B) Genotyping of tissues from *Lin9*$^{fl/fl}$ *CreER*^{T2} mice treated with tamoxifen by intraperitonal injection for three consecutive days. Two- to 3-month-old *Lin9*$^{+/+}$ *CreER*^{T2} or *Lin9*$^{fl/fl}$ *CreER*^{T2} mice were treated with tamoxifen. The intestinal phenotype was analyzed at the indicated day (d) after the first injection. (Upper panel) H&E staining showing normal crypt-villus morphology in the duodenum of *Lin9*$^{+/+}$ *CreER*^{T2} animals. (Lower panels) Intestinal epithelium atrophy after deletion of *Lin9* in *Lin9*$^{fl/fl}$ *CreER*^{T2} mice. (C) Intestinal epithelium atrophy is associated with the loss of proliferating cells. Mice were treated with tamoxifen as described above. At the indicated time points after the first tamoxifen injection, proliferation was analyzed by staining for the proliferation marker Ki-67. (D) Four days after the first tamoxifen injection, mice were injected with BrdU for 2 h to label proliferating cells. The percentage of BrdU-positive cells was analyzed by staining with a BrdU antibody (E) Abnormal nuclei

per crypt. After deletion of *Lin9* there were significantly fewer BrdU-positive cells in crypts of $Lin9^{fl/fl}$ $CreER^{T2}$ mice. In addition, we observed crypt cells and villus enterocytes with abnormal nuclei after deletion of *Lin9*. Abnormalities included large and irregular nuclei as well as binucleated cells (Fig. 7E). Morphometrical analysis confirmed an increased nuclear area of villus enterocytes (Fig. 7E). The increase in nuclear area and the presence of binuclear cells could reflect changes in genomic stability, such as aneuploidy and polyploidy and cytokinesis failure. In support of this possibility, we observed that mitotic gene expression was strongly reduced in the intestines of $Lin9^{fl/fl}$ $CreER^{T2}$ animals treated with tamoxifen, indicating that LIN9 is required to maintain mitotic gene expression *in vivo* (Fig. 7F).

Mitotic checkpoint defect and transformation of *Lin9* heterozygous MEFs. As described above, *Lin9* heterozygous mice develop normally and have no obvious phenotype. Similarly, a reduction of *Lin9* to about 50% in 4-OHT-treated heterozygous $Lin9^{fl/+}$ $CreER^{T2}$ MEFs had no significant effect on cell proliferation and did not result in binuclear cells, although expression of mitotic genes was slightly reduced (Fig. 8A, B, and C). However, when cells were treated with the spindle poison nocodazole to activate the spindle checkpoint, the percentage of cells arrested in mitosis was reduced in 4-OHT-treated heterozygous MEFs compared to wild-type cells (Fig. 8D). This indicates that the mitotic checkpoint of *Lin9* heterozygous MEFs is weakened. We next asked whether the mitotic spindle defect of $Lin9^{+/-}$ MEFs contributes to oncogenic transformation *in vitro*. First, primary $Lin9^{fl/+}$ $CreER^{T2}$ MEFs were immortalized with the SV40 large T antigen (LT), generating $Lin9^{fl/+}$ $CreER^{T2}$(LT) cells. Importantly, SV40 large T is not sufficient to transform MEFs (17, 36). Because SV40 large T interferes with the spindle checkpoint by interacting with the mitotic spindle checkpoint protein Bub1, we also used a mutant of large T (LTΔ89–97) defective for Bub1 binding (5). Next, the ability of $Lin9^{fl/+}$ $CreER^{T2}$(LT) and (LTΔ89–97) cells to grow independent of anchorage in soft agar was analyzed. $Lin9^{fl/+}$ $CreER^{T2}$(LT) and (LTΔ89–97) cells that had not been treated with 4-OHT only formed a low number of background colonies, as expected (Fig. 8E). In striking contrast, 4-OHT-treated $Lin9^{fl/+}$ $CreER^{T2}$(LT) and (LTΔ89–97) cells formed a high number of rapidly growing colonies, indicating that *Lin9* heterozygosity promotes anchorage-independent growth (Fig. 8E).

***Lin9* heterozygosity shortens the life span and accelerates lung tumor growth in Raf-BXB transgenic mice.** Next we tested whether *Lin9* heterozygosity contributes to tumorigenesis *in vivo* upon challenge with an oncogene. To address this possibility, we tested the effect of *Lin9* heterozygosity in a model of non-small-cell lung tumorigenesis in mice that express a constitutively active c-*raf-1* kinase under the control of the human SP-C promoter (BXB-Raf) (18). To examine the effect of loss of one allele of *Lin9* on BXB-Raf-induced lung adenoma formation, BXB-Raf mice were crossed with $Lin9^{+/-}$ mice. BXB-Raf mice develop multiple benign lung adenomas within 3 months after birth and they die after more than 1 year. *Lin9* heterozygosity significantly shortened the life span of BXB-Raf mice (Fig. 8F). After 370 days, only two of the $Lin9^{+/+}$BXB-Raf mice had died. In contrast, in the same time span, 11 of 19 $Lin9^{+/-}$ BXB-Raf animals had died ($P = 0.013$). Histological examination and morphometric analysis at 4 to 5 months showed that the number of tumors and total tumor area were increased in *Lin9* heterozygous animals (Fig. 8G, H, and I). $Lin9^{+/-}$ BXB-Raf animals developed about twice as many lung tumors as $Lin9^{+/+}$ BXB-Raf mice. Proliferation of tumor cells was equivalent as determined by Ki67 staining, and no differences in the expression of differentiation and progression markers were observed in tumors from $Lin9^{+/+}$ BXB-Raf and $Lin9^{+/-}$ BXB-Raf mice (data not shown). In conclusion, *Lin9* heterozygosity cooperates with oncogenic Raf in tumor initiation, possibly due to altered genomic stability.

DISCUSSION

The primary aim of this study was to elucidate the *in vivo* function of the mammalian DREAM/LINC complex. To this end we used classical and conditional knockout strategies to inactivate *Lin9*, a conserved key subunit of DREAM/LINC. We discovered that LIN9 has nonredundant functions and that it is essential for early embryonic development and for viability of adult mice.

Since *Lin9* mutant embryos die at the peri-implantation stage and fail to maintain an ICM *in vitro*, it is possible that *Lin9* is required for stem cell expansion by regulating the levels of pluripotency genes. In favor of this hypothesis, B-MYB, which interacts with DREAM/LINC in S phase, has been implicated in expression of the stem cell pluripotency factor *Oct4* (45). Furthermore, like $Lin9^{-/-}$ mice, *B-Myb* mutant mice die at the peri-implantation stage and show defects in ICM formation *in vitro* (44). However, we found that levels of pluripotency factors were unchanged in *Lin9*-depleted ES cells (data not shown). We therefore favor the hypothesis that the phenotype of *Lin9* mutant embryos is due to defects in cell division, based on our findings that *Lin9* is required for mitosis and cytokinesis (see below) and the results of Knight et al. that showed that LIN9 and B-MYB regulated G_2/M genes in embryonic carcinoma cells (20).

We found that deletion of *Lin9* in MEFs resulted in rapid loss of proliferation and was associated with multiple defects in mitosis and failure of cytokinesis. These phenotypes can be readily explained by the reduced expression of G_2/M genes upon loss of *Lin9.* For instance, Plk1 and Aurora A are major mitotic kinases and Kif20a and Kif23 are essential for cytokinesis (8, 10, 30). Interestingly, levels of proteins that participate in the spindle checkpoint and maintain chromosomal stability, such as Cenp-e, were also reduced in *Lin9*-deficient

in the intestinal epithelium upon deletion of *Lin9*. (Right) Morphometric analysis of nuclear size. The mean nuclear diameter of villus enterocytes increased from 23.19 μm^2 to 30.14 μm^2 ($P < 0.0001$). (F) *Lin9* was deleted by three consecutive daily intraperitoneal injections of 1 mg of tamoxifen into $Lin9^{fl/fl}$ $CreER^{T2}$ mice. Three and four days after the first injection, RNA was isolated from the intestine. Levels of the indicated mitotic genes were analyzed by real time RT-PCR.

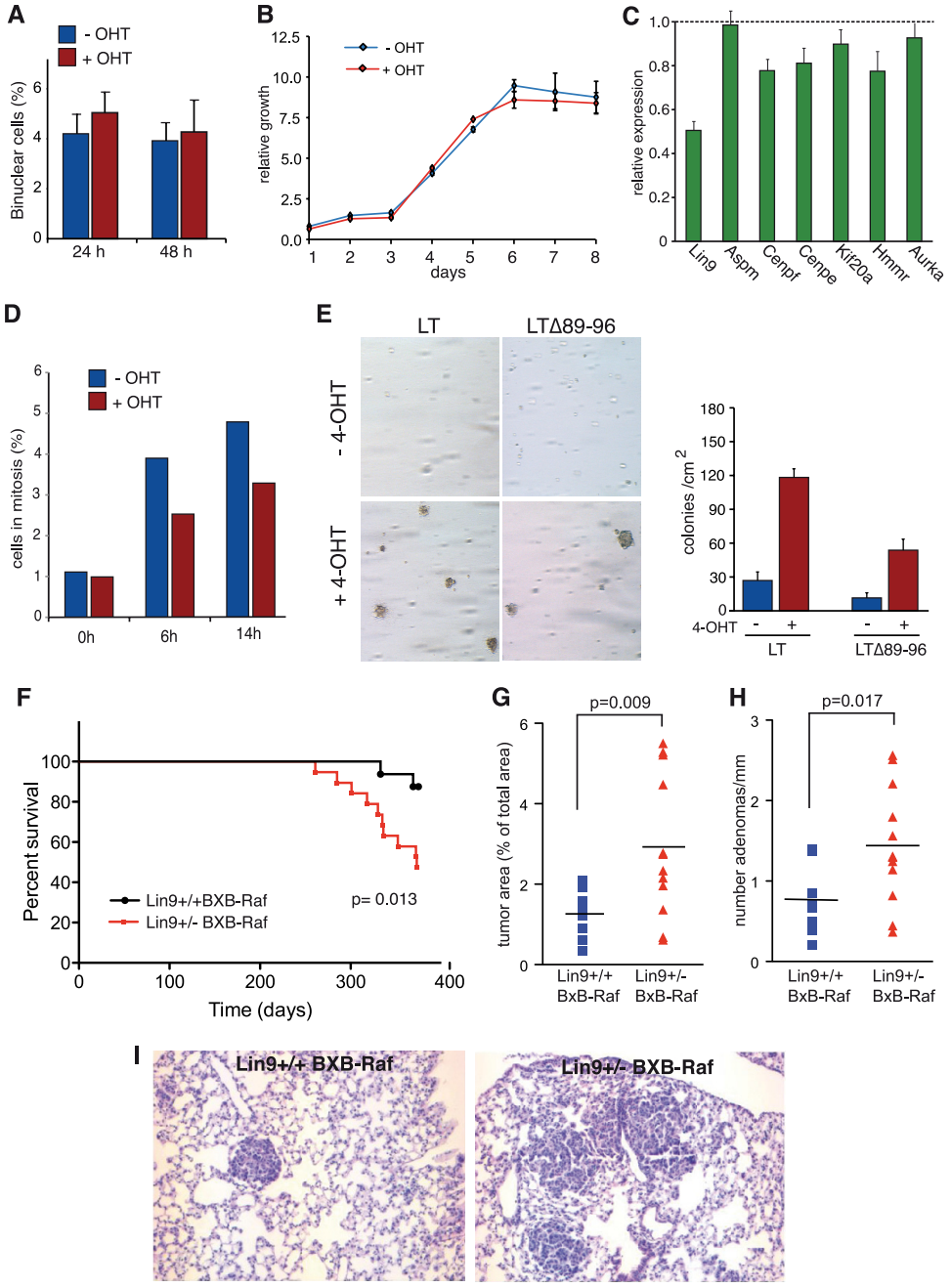

FIG. 8. *Lin9* heterozygosity leads to a weakened spindle checkpoint and contributes to tumorigenicity in a model of non-small-cell lung cancer. (A) $Lin9^{fl/+}$ $CreER^{T2}$ MEFs were treated with 4-OHT or untreated. At the indicated times after treatment the percentage of binuclear cells was determined. (B) Growth of 4-OHT-treated and untreated $Lin9^{fl/+}$ $CreER^{T2}$ MEFs was analyzed. (C) Gene expression in $Lin9^{fl/+}$ $CreER^{T2}$ MEFs was analyzed by qPCR. Data show expression in 4-OHT-treated cells relative to untreated cells. (D) Mitotic index of untreated and 4-OHT-treated $Lin9^{fl/+}$ $CreER^{T2}$ MEFs following treatment with nocodazole for the indicated time periods. The experiment was repeated several times. One representative experiment is shown. (E) *Lin9* heterozygosity results in growth in soft agar. $Lin9^{fl/+}$ $CreER^{T2}$ MEFs were immortalized with SV40(LT) or (LTΔ89–96). After treatment with 4-OHT to delete *Lin9*, cells formed colonies in soft agar. (Right) Number of colonies in 4-OHT-treated and untreated samples. (F) Reduced survival of *Lin9* heterozygous mice in a model of small cell lung cancer. The Kaplan-Meier plot shows survival of $Lin9^{+/+}$ BXB-Raf and $Lin9^{+/-}$ BXB-Raf mice. *P* values were calculated using the log-rank test. (G and H) Quantification of tumor area (G) and tumor incidence (H) in SP-C $Lin9^{+/+}$ BXB-Raf and $Lin9^{+/-}$ BXB-Raf lungs from 4- to 5-month-old animals. Medians are indicated by the horizontal lines. *P* values were calculated using Student's *t* test. (I) H&E staining of lung sections from $Lin9^{+/+}$ BXB-Raf and $Lin9^{+/-}$ BXB-Raf mice.

cells. Many of the LIN9-regulated mitotic genes, such as Plk1, Cenp-a, and Fbxo5/Emi1, are essential for mouse embryogenesis, suggesting that the lethality of *Lin9* mutant embryos is due to loss of expression of one or more of these genes (15, 22, 26). The timing of developmental arrest may reflect the stage at which the maternally produced LIN9 gene product is depleted.

The essential role for *Lin9* is not limited to embryogenesis. Loss of *Lin9* in adult mice resulted in atrophy of the intestinal

epithelium and in rapid death of the animals. Intestinal epithelium atrophy was associated with loss of proliferation and the accumulation of binuclear and abnormal nuclei, indicating that *Lin9* is also necessary for proper execution of mitosis in dividing adult tissues. The ability of LINC/DREAM to function as a key regulator of G_2/M genes is evolutionarily conserved and has also been observed in flies and zebrafish (13, 19).

ChIP experiments showed binding of LIN9 to the promoters of mitotic genes, suggesting that they are direct *in vivo* targets of the mammalian DREAM/LINC complex. The DNA binding proteins LIN54 and B-MYB could be—either alone or together—responsible for recruiting the complex to DNA. This is consistent with the known roles of B-MYB and LIN54 in transcription of G_2 genes (39, 47). How DREAM–B-MYB activates mitotic genes remains to be determined, because no chromatin-modifying enzymes have been detected in association with the human complex. Loss of LIN9 was associated with reduced trimethylation of histone H3 lysine 4 at target promoters, suggesting the possible recruitment of a histone methyltransferase of the mixed lineage leukemia or SET family.

DREAM/LINC associates with p130/E2F4 in repressors in quiescent cells and has been implicated in repression of E2F target genes (25). Unexpectedly, we found that p130/E2F4-repressed genes were unaffected by the loss of *Lin9*. Consistent with this finding, entry into the cell cycle was unchanged in *Lin9* knockout MEFs compared to wild-type cells, while it occurred earlier in *p130/p107* MEFs (16). This argues that repression by p130/E2F4 is independent of LIN9, although it is possible that other subunits of DREAM/LINC are involved in p130/E2F4-mediated repression.

Although we found that complete loss of *Lin9* inhibits proliferation of primary and immortalized cells, *Lin9* heterozygosity contributed to transformation of immortalized MEFs. Similarly, while *Lin9* haploinsufficient mice are not predisposed to spontaneous tumorigenesis, $Lin9^{+/-}$ mice develop lung adenomas at an increased rate in an *in vivo* model of lung tumorigenesis induced by the c-*raf* oncogene. Since *Lin9* is required for a robust spindle checkpoint, it is possible that decreased *Lin9* expression contributes to transformation by causing genomic instability. This is consistent with studies of mitotic checkpoint genes in mice, which, in many cases, did not show an increase in spontaneous tumorigenesis in heterozygous animals but an increased risk for carcinogen-induced tumors (1, 6). This suggests that cooperating oncogenes are necessary to synergize with failure of the mitotic spindle checkpoint during tumorigenesis. Because we previously observed that LIN9 promotes differentiation together with pRB (11), this function of LIN9 could also limit the ability of Raf1 to transform cells. Deletion of one allele of *Lin9* may thus sensitize cells to Raf1-mediated transformation. Either mechanism may be relevant to tumor formation in humans.

ACKNOWLEDGMENTS

We thank all members of the laboratory for their suggestions and critical reading of the manuscript. We thank Susanne Spahr for her excellent technical assistance, Michael Krause and Birgit Samans for microarray analysis, Anton Berns for providing $CreER^{T2}$ mice, Susan Dymecki for FLPe mice, Imme Krüger and Guntram Suske for help with constructing the targeting vector, Thorsten Stiewe and Ole Gjoerup for large T constructs, Daniel Murphy for assistance with immunohistochemistry, and Andreas Hock and Tim Krüger for help with the time lapse experiments.

This work was supported by grants from the DFG (575/5-1 and TR17-B1) to S.G.

REFERENCES

1. **Baker, D. J., K. B. Jeganathan, L. Malureanu, C. Perez-Terzic, A. Terzic, and J. M. van Deursen.** 2006. Early aging-associated phenotypes in Bub3/Rae1 haploinsufficient mice. J. Cell Biol. **172:**529–540.
2. **Beall, E. L., M. Bell, D. Georlette, and M. R. Botchan.** 2004. Dm-myb mutant lethality in Drosophila is dependent upon mip130: positive and negative regulation of DNA replication. Genes Dev. **18:**1667–1680.
3. **Beitel, G. J., E. J. Lambie, and H. R. Horvitz.** 2000. The C. elegans gene lin-9, which acts in an Rb-related pathway, is required for gonadal sheath cell development and encodes a novel protein. Gene **254:**253–263.
4. **Bernstein, B. E., M. Kamal, K. Lindblad-Toh, S. Bekiranov, D. K. Bailey, D. J. Huebert, S. McMahon, E. K. Karlsson, E. J. Kulbokas, 3rd, T. R. Gingeras, S. L. Schreiber, and E. S. Lander.** 2005. Genomic maps and comparative analysis of histone modifications in human and mouse. Cell **120:**169–181.
5. **Cotsiki, M., R. L. Lock, Y. Cheng, G. L. Williams, J. Zhao, D. Perera, R. Freire, A. Entwistle, E. A. Golemis, T. M. Roberts, P. S. Jat, and O. V. Gjoerup.** 2004. Simian virus 40 large T antigen targets the spindle assembly checkpoint protein Bub1. Proc. Natl. Acad. Sci. U. S. A. **101:**947–952.
6. **Dai, W., Q. Wang, T. Liu, M. Swamy, Y. Fang, S. Xie, R. Mahmood, Y. M. Yang, M. Xu, and C. V. Rao.** 2004. Slippage of mitotic arrest and enhanced tumor development in mice with BubR1 haploinsufficiency. Cancer Res. **64:**440–445.
7. **DeGregori, J., and D. G. Johnson.** 2006. Distinct and overlapping roles for E2F family members in transcription, proliferation and apoptosis. Curr. Mol. Med. **6:**739–748.
8. **Eggert, U. S., T. J. Mitchison, and C. M. Field.** 2006. Animal cytokinesis: from parts list to mechanisms. Annu. Rev. Biochem. **75:**543–566.
9. **Fay, D. S., and M. Han.** 2000. The synthetic multivulval genes of C. elegans: functional redundancy, Ras-antagonism, and cell fate determination. Genesis **26:**279–284.
10. **Fu, J., M. Bian, Q. Jiang, and C. Zhang.** 2007. Roles of Aurora kinases in mitosis and tumorigenesis. Mol. Cancer Res. **5:**1–10.
11. **Gagrica, S., S. Hauser, I. Kolfschoten, L. Osterloh, R. Agami, and S. Gaubatz.** 2004. Inhibition of oncogenic transformation by mammalian Lin-9, a pRB-associated protein. EMBO J. **23:**4627–4638.
12. **Gaubatz, S., G. J. Lindeman, S. Ishida, L. Jakoi, J. R. Nevins, D. M. Livingston, and R. E. Rempel.** 2000. E2F4 and E2F5 play an essential role in pocket protein-mediated G_1 control. Mol. Cell **6:**729–735.
13. **Georlette, D., S. Ahn, D. M. MacAlpine, E. Cheung, P. W. Lewis, E. L. Beall, S. P. Bell, T. Speed, J. R. Manak, and M. R. Botchan.** 2007. Genomic profiling and expression studies reveal both positive and negative activities for the Drosophila Myb MuvB/dREAM complex in proliferating cells. Genes Dev. **21:**2880–2896.
14. **Harrison, M. M., C. J. Ceol, X. Lu, and H. R. Horvitz.** 2006. Some C. elegans class B synthetic multivulva proteins encode a conserved LIN-35 Rb-containing complex distinct from a NuRD-like complex. Proc. Natl. Acad. Sci. U. S. A. **103:**16782–16787.
15. **Howman, E. V., K. J. Fowler, A. J. Newson, S. Redward, A. C. MacDonald, P. Kalitsis, and K. H. Choo.** 2000. Early disruption of centromeric chromatin organization in centromere protein A (Cenpa) null mice. Proc. Natl. Acad. Sci. U. S. A. **97:**1148–1153.
16. **Hurford, R. K., Jr., D. Cobrinik, M. H. Lee, and N. Dyson.** 1997. pRB and p107/p130 are required for the regulated expression of different sets of E2F responsive genes. Genes Dev. **11:**1447–1463.
17. **Jat, P. S., and P. A. Sharp.** 1986. Large T antigens of simian virus 40 and polyomavirus efficiently establish primary fibroblasts. J. Virol. **59:**746–750.
18. **Kerkhoff, E., L. M. Fedorov, R. Siefken, A. O. Walter, T. Papadopoulos, and U. R. Rapp.** 2000. Lung-targeted expression of the c-Raf-1 kinase in transgenic mice exposes a novel oncogenic character of the wild-type protein. Cell Growth Differ. **11:**185–190.
19. **Kleinschmidt, M. A., T. U. Wagner, D. Liedtke, S. Spahr, B. Samans, and S. Gaubatz.** 2009. lin9 is required for mitosis and cell survival during early zebrafish development. J. Biol. Chem. **284:**13119–13127.
20. **Knight, A. S., M. Notaridou, and R. J. Watson.** 2009. A Lin-9 complex is recruited by B-Myb to activate transcription of G(2)/M genes in undifferentiated embryonal carcinoma cells. Oncogene **28:**1737–1747.
21. **Korenjak, M., and A. Brehm.** 2005. E2F-Rb complexes regulating transcription of genes important for differentiation and development. Curr. Opin. Genet. Dev. **15:**520–527.
22. **Lee, H., D. J. Lee, S. P. Oh, H. D. Park, H. H. Nam, J. M. Kim, and D. S. Lim.** 2006. Mouse emi1 has an essential function in mitotic progression during early embryogenesis. Mol. Cell. Biol. **26:**5373–5381.
23. **Leimeister, C., N. Schumacher, C. Steidl, and M. Gessler.** 2000. Analysis of

HeyL expression in wild-type and Notch pathway mutant mouse embryos. Mech. Dev. **98:**175–178.
24. **Lewis, P. W., E. L. Beall, T. C. Fleischer, D. Georlette, A. J. Link, and M. R. Botchan.** 2004. Identification of a Drosophila Myb-E2F2/RBF transcriptional repressor complex. Genes Dev. **18:**2929–2940.
25. **Litovchick, L., S. Sadasivam, L. Florens, X. Zhu, S. K. Swanson, S. Velmurugan, R. Chen, M. P. Washburn, X. S. Liu, and J. A. DeCaprio.** 2007. Evolutionarily conserved multisubunit RBL2/p130 and E2F4 protein complex represses human cell cycle-dependent genes in quiescence. Mol. Cell **26:**539–551.
26. **Lu, L. Y., J. L. Wood, K. Minter-Dykhouse, L. Ye, T. L. Saunders, X. Yu, and J. Chen.** 2008. Polo-like kinase 1 is essential for early embryonic development and tumor suppression. Mol. Cell. Biol. **28:**6870–6876.
27. **Mountford, P., B. Zevnik, A. Duwel, J. Nichols, M. Li, C. Dani, M. Robertson, I. Chambers, and A. Smith.** 1994. Dicistronic targeting constructs: reporters and modifiers of mammalian gene expression. Proc. Natl. Acad. Sci. U. S. A. **91:**4303–4307.
28. **Nichols, J., B. Zevnik, K. Anastassiadis, H. Niwa, D. Klewe-Nebenius, I. Chambers, H. Schöler, and A. Smith.** 1998. Formation of pluripotent stem cells in the mammalian embryo depends on the POU transcription factor Oct4. Cell **95:**379–391.
29. **Osterloh, L., B. von Eyss, F. Schmit, L. Rein, D. Hubner, B. Samans, S. Hauser, and S. Gaubatz.** 2007. The human synMuv-like protein LIN-9 is required for transcription of G_2/M genes and for entry into mitosis. EMBO J. **26:**144–157.
30. **Petronczki, M., P. Lenart, and J. M. Peters.** 2008. Polo on the rise: from mitotic entry to cytokinesis with Plk1. Dev. Cell **14:**646–659.
31. **Pilkinton, M., R. Sandoval, and O. R. Colamonici.** 2007. Mammalian Mip/LIN-9 interacts with either the p107, p130/E2F4 repressor complex or B-Myb in a cell cycle-phase-dependent context distinct from the Drosophila dREAM complex. Oncogene **29:**7535–7543.
32. **Pilkinton, M., R. Sandoval, J. Song, S. A. Ness, and O. R. Colamonici.** 2007. Mip/LIN-9 regulates the expression of B-Myb and the induction of cyclin A, cyclin B, and CDK1. J. Biol. Chem. **282:**168–175.
33. **Poirier, F., C. T. Chan, P. M. Timmons, E. J. Robertson, M. J. Evans, and P. W. Rigby.** 1991. The murine H19 gene is activated during embryonic stem cell differentiation in vitro and at the time of implantation in the developing embryo. Development **113:**1105–1114.
34. **Rapp, U. R., C. Korn, F. Ceteci, C. Karreman, K. Luetkenhaus, V. Serafin, E. Zanucco, I. Castro, and T. Potapenko.** 2009. MYC is a metastasis gene for non-small-cell lung cancer. PLoS One **4:**e6029.
35. **Rodriguez, C. I., F. Buchholz, J. Galloway, R. Sequerra, J. Kasper, R. Ayala, A. F. Stewart, and S. M. Dymecki.** 2000. High-efficiency deleter mice show that FLPe is an alternative to Cre-loxP. Nat. Genet. **25:**139–140.
36. **Rundell, K., and R. Parakati.** 2001. The role of the SV40 ST antigen in cell growth promotion and transformation. Semin. Cancer Biol. **11:**5–13.
37. **Sandoval, R., J. Xue, X. Tian, K. Barrett, M. Pilkinton, D. S. Ucker, P. Raychaudhuri, R. D. Kineman, R. M. Luque, G. Baida, X. Zou, V. E. Valli, J. L. Cook, H. Kiyokawa, and O. R. Colamonici.** 2006. A mutant allele of BARA/LIN-9 rescues the cdk4-/- phenotype by releasing the repression on E2F-regulated genes. Exp. Cell Res. **312:**2465–2475.
38. **Sauer, B.** 1993. Manipulation of transgenes by site-specific recombination: use of Cre recombinase. Methods Enzymol. **225:**890–900.
39. **Schmit, F., S. Cremer, and S. Gaubatz.** 2009. LIN54 is an essential core subunit of the DREAM/LINC complex that binds to the cdc2 promoter in a sequence-specific manner. FEBS J. **276:**5703–5716.
40. **Schmit, F., M. Korenjak, M. Mannefeld, K. Schmitt, C. Franke, B. V. Eyss, S. Gagrica, F. Hanel, A. Brehm, and S. Gaubatz.** 2007. LINC, a human complex that is related to pRB-containing complexes in invertebrates regulates the expression of G_2/M genes. Cell Cycle **6:**1903–1913.
41. **Schneider, R., A. J. Bannister, F. A. Myers, A. W. Thorne, C. Crane-Robinson, and T. Kouzarides.** 2004. Histone H3 lysine 4 methylation patterns in higher eukaryotic genes. Nat. Cell Biol. **6:**73–77.
42. **Schwenk, F., U. Baron, and K. Rajewsky.** 1995. A cre-transgenic mouse strain for the ubiquitous deletion of loxP-flanked gene segments including deletion in germ cells. Nucleic Acids Res. **23:**5080–5081.
43. **Serrano, M.** 1997. The tumor suppressor protein p16INK4a. Exp. Cell Res. **237:**7–13.
44. **Tanaka, Y., N. P. Patestos, T. Maekawa, and S. Ishii.** 1999. B-myb is required for inner cell mass formation at an early stage of development. J. Biol. Chem. **274:**28067–28070.
45. **Tarasov, K. V., Y. S. Tarasova, W. L. Tam, D. R. Riordon, S. T. Elliott, G. Kania, J. Li, S. Yamanaka, D. G. Crider, G. Testa, R. A. Li, B. Lim, C. L. Stewart, Y. Liu, J. E. Van Eyk, R. P. Wersto, A. M. Wobus, and K. R. Boheler.** 2008. B-MYB is essential for normal cell cycle progression and chromosomal stability of embryonic stem cells. PLoS One **3:**e2478.
46. **Vooijs, M., J. Jonkers, and A. Berns.** 2001. A highly efficient ligand-regulated Cre recombinase mouse line shows that LoxP recombination is position dependent. EMBO Rep. **2:**292–297.
47. **Zhu, W., P. H. Giangrande, and J. R. Nevins.** 2004. E2Fs link the control of G_1/S and G_2/M transcription. EMBO J. **23:**4615–4626.